JOURNAL OF CATALYSIS 147, 322–332 (1994)

Effects of Oxygen Vacancy of Yttria-Stabilized Zirconia Support on Carbon Monoxide Oxidation over Copper Catalyst

Wei-Ping Dow and Ta-Jen Huang[1]

Department of Chemical Engineering, National Tsing Hua University, Hsinchu, Taiwan 300, Republic of China

Received October 25, 1993; revised January 13, 1994

CO oxidation activity was measured at atmospheric pressure and at temperatures of 300 to 450°C over copper catalysts supported on 6.8 mol% yttria-stabilized zirconia (YSZ). Fresh, high-temperature reduced with CO, and reoxidized catalysts were investigated using two reacting atmospheres, oxygen lean and oxygen rich. Temperature-programmed reduction using CO as reducing gas was employed to characterize the dispersion and the copper oxide species of catalysts before and after the reaction. Results were discussed in light of the occupancy of surface oxygen vacancies of YSZ support by copper atoms, the penetration of copper atoms into bulk oxygen vacancies of YSZ support, and the interfacial Cu_2O formation owing to surface oxygen vacancies of YSZ support. These also suggest that geometric interfacial metal–support interaction can enhance the activity of copper catalyst by improving the dispersion and stabilizing the interfacial Cu_2O through the oxygen vacancies of support. A mechanism in which oxygen vacancies of YSZ support can protect the interfacial Cu_2O to avoid further reduction or oxidation has been proposed. The occurrence of penetration, redispersion, and split of copper species crystallites has also been explained by an oxygen vacancy model. © 1994 Academic Press, Inc.

1. INTRODUCTION

Metal–support interaction in catalytic reactions over supported metal catalysts has received considerable attention over the past years. Strong metal–support interaction (SMSI) (1) and interfacial metal–support interaction (IMSI) (2, 3) are two dominant and marked subjects in this field. These interactions are investigated mostly on group VIII metals supported on reducible metal oxides (e.g., TiO_2) (1, 4–6). Owing to the reducibility of supports, many studies (1, 4–6) suggest that SMSI is due to an electronic effect. However, the electronic model fails as the particle size of supported metal becomes large. On the other hand, the geometric model of IMSI is successful in explaining those phenomena of metal–support interaction. Burch and Flambard (2) propose an IMSI model that suggests that oxygen vacancy of support is the active site. This model has been extensively applied to CO hydrogenation (2, 7) and CO oxidation (8–11).

Recently, Ekerdt and co-workers (12, 13) confirmed that the active site for CO hydrogenation over ZrO_2 or Y_2O_3-doped ZrO_2 is an oxygen anion vacancy. Sanchez and Gazquez (14) and Shpiro *et al.* (15) also propose that SMSI is due to the oxygen vacancy of support, which causes a geometric effect that can affect the dispersion and alter the morphology of supported metal. In addition, Cho (16) demonstrates that the oxygen vacancies of Gd_2O_3-doped CeO_2 support can significantly enhance the catalytic activity of Rh for the NO + CO reaction.

Sanchez and Gazquez (14) classified the oxide supports into two types, i.e., fluorite-type and rutile-type oxide. For the fluorite-type oxide (e.g., ZrO_2), interactions are mainly limited to metal occupancy of surface vacancies. Consequently, this interaction leads to high metal dispersion, high catalytic activity, and unusual stability against sintering. On the rutile-type oxide (e.g., TiO_2), metal may diffuse into support bulk vacancies and metal burial is possible. Consequently, a decrease in chemisorptive capacity of metal may be observed. The loss of sorptive and catalytic properties is not attributed to the charge transfer between metal and support but to the geometric effect.

The purpose of this work is to elucidate the importance of oxygen vacancy of support, which causes a geometric factor, on metal–support interaction. Hence, the support employed in this study must be free of electronic factor. Yttria-stabilized zirconia (YSZ) was employed since it, being an outstanding oxygen-ion conductor, has been extensively used as a solid electrolyte for fuel cells, oxygen sensors, etc. (17, 18), and its electronic transport number is almost equal to zero (17, 19). Hence, electron transfer between metal and YSZ support can be neglected (3). In addition, the oxygen vacancies of YSZ are inborn (17, 19). This is different with rutile-type oxide, of which oxygen vacancies are created by pretreatment of high-temperature reduction (HTR).

For CO oxidation, noble metal catalysts such as Pt and Pd have been demonstrated to be very effective (20).

[1] To whom correspondence should be addressed.

0021-9517/94 $6.00

However, attention has also been given to base metals, especially copper oxide (21, 22), due to the limited availability of precious metals. During CO oxidation, copper oxide can exhibit activities per unit surface area similar to those of noble-metal catalysts such as platinum (23). Unfortunately, sintering is usually a problem for copper catalysts in automobile emission control (23, 24). Therefore, this work studies the effects of oxygen vacancies of YSZ support on sintering, dispersion, and valence of copper oxide during CO oxidation. Results show that oxygen vacancies of YSZ support can improve dispersion of the copper species and cause the formation of interfacial Cu_2O which leads to activity enhancement.

2. EXPERIMENTAL

Catalysts were prepared by impregnating γ-alumina (Strem, 150–200 mesh) and 6.8 mol% YSZ (Cerac, 5.6 μm) with an appropriate amount of aqueous solution of copper nitrate (Strem, 99.999%). After evaporating the excess water at 80°C, the catalyst was dried in air for 24 h at 120°C and then calcined in air for 3.5 h at 500°C, which was raised from room temperature at a rate of 10°C/min. The fresh catalyst as defined in this work is the catalyst that underwent the above steps without further treatment. Cu/YSZ (1 wt%) (nominal composition by weight of the reduced catalyst) was chosen to characterize the copper content and to confirm the accuracy of the preparation method; 0.5 g of 1 wt% Cu/YSZ was dissolved in 20 ml HNO_3 solution and the resulting solution was diluted by deionized water. It was then analyzed by atomic absorption spectrometer (Varian, model Spectra A-30) and the composition was found to be 0.97 wt% Cu, which was very close to the indicated value of 1 wt% Cu.

The BET surface area of the catalyst was determined by means of nitrogen physisorption, applying a thermal conductivity detector (TCD) instrument (Quantachrome, U.S.A.). The copper surface area, which was used only for comparison with each other, was determined by applying a nitrous oxide pulse method as described by Evans *et al.* (25). Some comments on this method are described elsewhere (21). X-ray diffraction (XRD) spectra (Shimadzu, Model XD-5) was carried out using Cu$K_{\alpha 1}$ radiation. Samples for XRD were removed from the reactor after reaction, HTR, or reoxidation under an inert atmosphere at room temperature and then the XRD measurement was carried out immediately.

The activities of the catalyst were measured in a continuous flow reactor at atmospheric pressure and at a temperature of 300 to 450°C. The reactor was a 10-mm i.d. U-type quartz tube. The catalyst in the reactor was between 200 and 400 mg and not renewed when the temperature was raised to the next higher one. Before each activity test, the catalyst in the reactor was dried in ultrahigh-purity argon (99.9995%) at 300°C for 2 h in order to remove the hydroxyl groups or water adsorbed on the catalyst. HTR pretreatment was carried out with 5% CO in argon and a flow rate of 30 ml/min. The temperature was increased from room temperature to 800°C at the rate of 10°C/min and then held at 800°C for 30 min. Reoxidation treatment of catalyst was performed after HTR by passing an air flow for 1 h at 500°C. The CO oxidation activities presented in this work were taken after the set value of temperature was stable.

The flows of the reactant gases, CO (CP Grade, Air Products), O_2 (99.995%), and Ar (99.9995%), were adjusted by mass flow controllers (Hastings, Model HFC-202). Two reacting atmospheres, oxygen lean and oxygen rich, were adopted in this study. In the oxygen lean condition, the atmosphere consisted of 2% O_2, 6% CO, and the balance argon. In the oxygen rich condition, 4% O_2, 4% CO, and the balance argon were employed. The total flow rate of reactant mixture was 100 ml/min. The reactor outflow was analyzed on line by a gas chromatograph (Shimadzu, Model GC-8A), a CO-NDIR (nondispersive IR, Beckman, Model 880), and an oxygen analyzer (Beckman, Model 755A).

Temperature-programmed reduction (TPR) of the catalysts was carried out using either H_2 or CO as the reducing gas. H_2-TPR is employed to characterize the catalysts, while CO-TPR is carried out for the convenience of on-line analysis. The system and method of H_2-TPR was described elsewhere (26). The equipment of CO-TPR was the same as that of the activity test. Prior to each TPR run, the reactor was purged with ultrahigh-purity argon (99.9995%). The operating conditions of CO-TPR were similar to that of the HTR prereatment as mentioned above. The CO consumption in TPR was analyzed by CO-NDIR and its signal was transmited to a Y-t recorder (Yokogowa, Model LR-4110).

3. RESULTS

3.1. Surface Areas and TPR Characterization

The BET areas and copper surface areas of various catalysts are summarized in Table 1. The decrease in BET area of γ-alumina after calcination is presumably caused by the plugging of some micropores (27, 28) due to the loading of copper oxide. According to the particle size of YSZ powder, its BET area is mainly due to the external surface area. This implies that YSZ employed in this work is approximately nonporous.

Before activity test, catalysts have been characterized by TPR with hydrogen as the reducing gas, and the resulting TPR patterns are shown in Fig. 1. With YSZ as support, the peak temperature of TPR pattern of the catalyst with 1 wt% Cu is 250°C, while that with 5 wt% Cu is 274°C. Lower copper loading leading to lower peak

TABLE 1

Surface Areas of Various Catalysts

Catalysts or supports	BET Area (m^2/g)	Cu surface area (m^2/g)
YSZ	0.55	—
1 wt% Cu/YSZ	—	0.0452[a]
1 wt% Cu/YSZ	—	0.0306[b]
5 wt% Cu/YSZ	—	0.249[a]
5 wt% Cu/YSZ	—	0.185[b]
γ-alumina	235.4	—
1 wt% Cu/γ-alumina	189.1	0.073[a]
1 wt% Cu/γ-alumina	—	0.137[b]
5 wt% Cu/γ-alumina	180.9	2.8[a]
5 wt% Cu/γ-alumina	—	2.44[b]

[a] Measured after a prereduction at 300°C for 1 h.
[b] Measured after a prereduction at 400°C for 1 h.

TABLE 2

Types of Activity Test

Type	Composition of reactants	Pretreatment
I	2% O_2 + 6% CO	Fresh catalyst
II	2% O_2 + 6% CO	HTR[a]
III	4% O_2 + 4% CO	HTR[a]
IV	4% O_2 + 4% CO	Fresh catalyst

[a] The catalyst is reduced at 800°C with 5% CO/Ar.

temperature of TPR has also been found by Shimokawabe *et al.* over CuO/ZrO_2 catalyst (29). These authors have demonstrated that the lower peak temperature is due to the highly dispersed copper oxide with an octahedral environment. Robertson *et al.* (30) and Van der Grift *et al.* (31) have also concluded that copper oxide supported on silica carrier is more easily reduced as compared with unsupported copper oxide. The support appears to function purely as a dispersing agent, enhancing the reactivity of copper oxide towards reduction. Hence, the lower copper loading of 1 wt% Cu/YSZ should lead to a higher dispersion than that of 5 wt% Cu/YSZ and thus give a lower reducing temperature.

On the other hand, with γ-alumina as support, the catalyst with 1 wt% Cu has a higher peak temperature than that with 5 wt% Cu. This has also been found by Severino *et al.* (24) and is due to the surface spinel, i.e., $CuAl_2O_4$, being easily formed on 1 wt% Cu/γ-alumina (32, 33). With 5 wt% Cu, the dispersed copper oxide is predominant and thus the lower peak temperature is observed during the TPR.

3.2. Catalytic Activities

The activity tests are divided into four types. In the type I test, the catalyst is fresh and the operating condition is oxygen lean. In the type II test, the catalyst has undergone a HTR pretreatment and the operating condition is also oxygen lean. In the type III test, the catalyst has also undergone a HTR pretreatment but the operating condition is oxygen rich. Finally, in the type IV test, the catalyst is fresh and the operating condition is also oxygen rich. These test types are listed in Table 2.

For comparison, the activity of 1 wt% Cu/γ-alumina measured under the type I test conditions is shown in Fig. 2 as a function of time-on-stream for different temperatures. It is seen that the activities are relatively stable for long periods of time at different temperatures.

Figure 3 shows the results of the type I test of 1 wt%

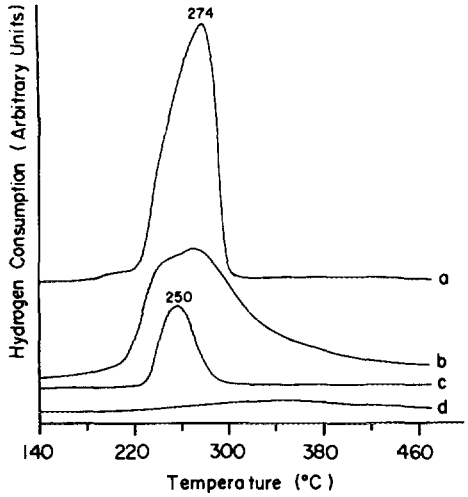

FIG. 1. TPR patterns. Operating conditions: 10°C/min, 10% H_2 in Ar with total flow rate of 30 ml/min, 200 mg of sample. Catalysis: (a) 5 wt% Cu/YSZ; (b) 5 wt% Cu/γ-alumina; (c) 1 wt% Cu/YSZ; (d) 1 wt% Cu/γ-alumina.

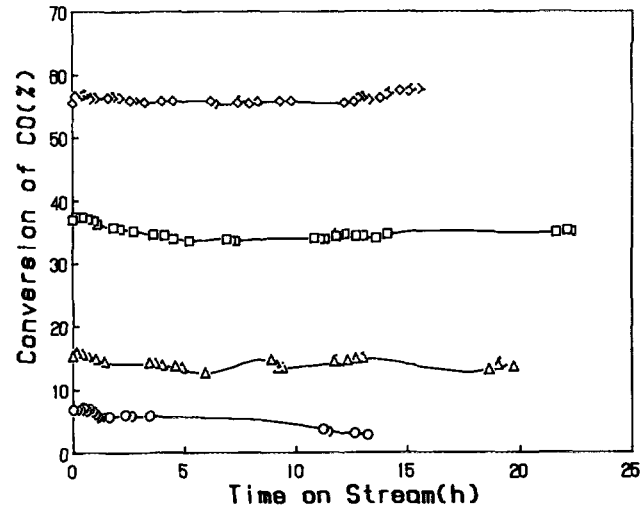

FIG. 2. Activity behavior of 1 wt% Cu/γ-alumina under the type I test. Sample, 200 mg. Temperatures: (○) 300°C; (△) 350°C; (□) 400°C; (◇) 450°C.

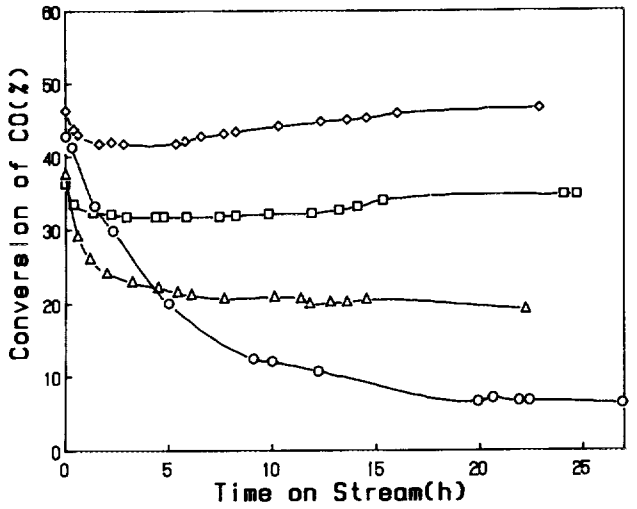

FIG. 3. Activity behavior of 1 wt% Cu/YSZ under the type I test. Sample 400 mg. Temperatures are as in Fig. 2.

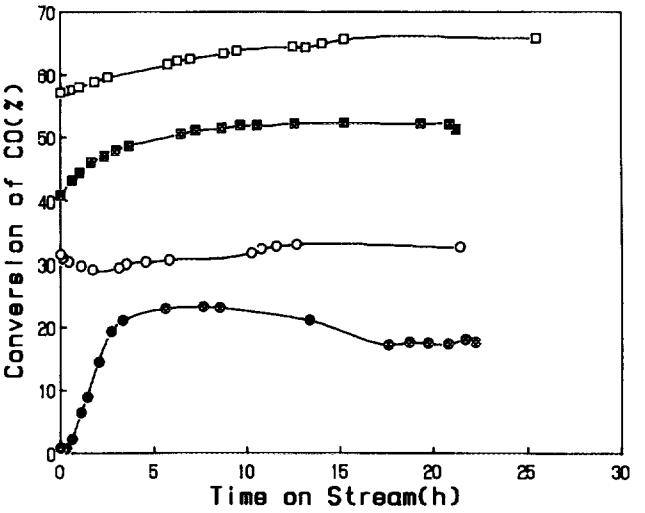

FIG. 5. Activity behavior of 1 wt% Cu/YSZ. Sample, 400 mg. Filled symbols, type III test; open symbols, type IV test. Temperature: circle, 300°C; square, 350°C.

Cu/YSZ. It is evident that a progressive deactivation is observed during the 300 and 350°C runs, especially at 300°C. However, a sustained increase in activity, even after 24 h, is observed when the reaction temperature is 400 or 450°C. Additionally, it is noted that deactivation always appears in the initial hours at 400 and 450°C.

Figure 4 shows the results of the type II test. The catalyst seems to be inert, even after 19 h, during the 300°C run. However, at 350°C, the activity rapidly appears and increases continuously. This sustained increase in activity with the run time at 350°C is contrary to that shown in Fig. 3, but the steady state activity is almost the same. Nevertheless, progressive deactivation is observed and the steady state activity is lower than that of Fig. 3 when the temperatures are 400 and 450°C.

Figure 5 shows the results of type III and type IV tests.

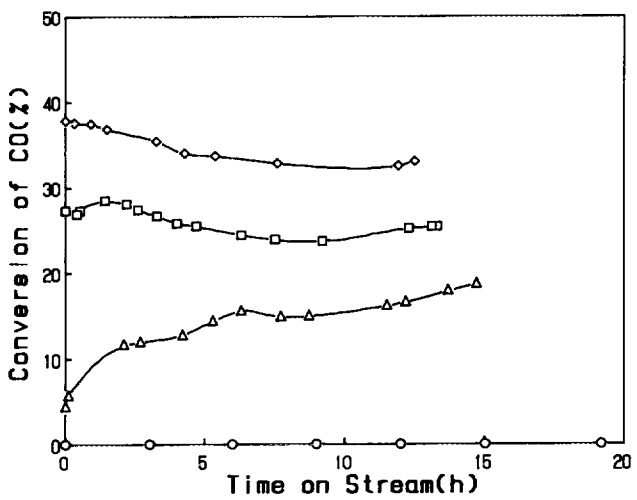

FIG. 4. Activity behavior of 1 wt% Cu/YSZ under the type II test. Sample, 400 mg. Temperatures are as in Fig. 2.

In the type III test at 300°C there is no detectable activity until 0.5 h. After 7 h, a mild deactivation is observed until 17 h, and then a steady state activity is observed. As the reaction temperature rises to 350°C, a sustained increase of activity is observed until 12 h. For the type IV test at 300 and 350°C the CO conversions exhibit a tendency to increase, especially at 350°C. From these results, it can be seen that the activities of 1 wt% Cu/YSZ are sensitive to the pretreatment and the gas phase condition during the run time. It is observed that the steady state activity of the type IV tested catalyst is always better than that of the type III tested one.

3.3 Temperature-Programmed Reduction

After each activity test, the CO-TPR of the sample was carried out. As shown in Fig. 6, the TPR peaks of the catalysts which were treated with type I and II tests at 450°C are much smaller but broader than that of the fresh catalyst. Moreover, the peak positions of the reaction-treated catalysts are at higher temperatures. In practice, it has been verified (34, 35) that the reducing temperature of cuprous oxide is higher than that of cupric oxide with a difference of 60°C or more. Hence, the CO consumption peaks of Figs. 6b and 6c can be attributed to cuprous oxide. It is interesting to note that three peaks were observed, as shown in Fig. 6d, after the catalyst had undergone the type I test at 300°C for 27 h. Again, the third peak (335°C) should also result from the cuprous oxide, but its amount is negligible. On the whole, the total CO consumption of the TPR pattern shown in Fig. 6d is much less than those of Figs. 6a, 6b, and 6c. This implies that most of the cupric oxide could be reduced to metallic copper after the type I test at 300°C for 27 h.

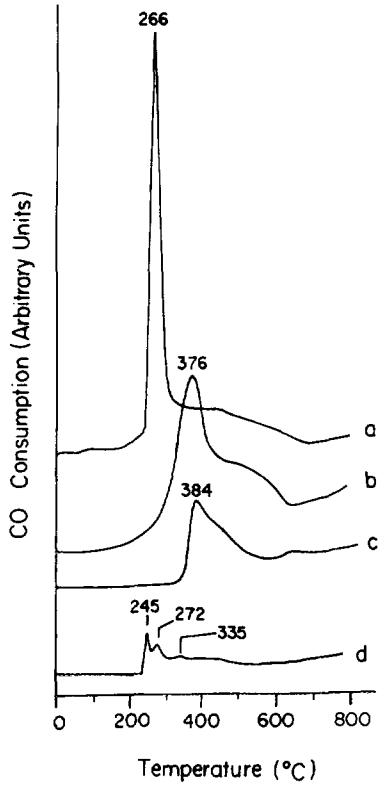

FIG. 6. TPR patterns of 1 wt% Cu/YSZ. Operating conditions: 10°C/min, 5% CO in Ar with total flow rate of 30 ml/min, 400 mg of sample. Pretreatment: (a) fresh; (b) type I test at 450°C; (c) type II test at 450°C; (d) type I test at 300°C.

As shown in Fig. 7, the peak profile of the type IV tested catalyst is very similar to that of the fresh catalyst (Fig. 6a) but has a shift of 13°C toward lower temperature. The TPR peak of the type III tested catalyst is smaller than that of the fresh catalyst and has a shift of 16°C toward higher temperature. The TPR of the catalyst which is reoxidized following HTR treatment has a large shift of 43°C toward lower temperature as compared with that of the fresh catalyst. It is believed that this 43°C difference is caused by the same oxide species, i.e., cupric oxide, with different dispersion and interaction between metal and support (29, 31, 36).

4. DISCUSSION

4.1. Sintering Behavior

With γ-alumina as support and low metal loading, the copper atom does not sinter easily due to the rough surface and the large BET area, but the surface spinel, $CuAl_2O_4$, is easily formed when the copper loading is lower than 4 wt% and the BET area is higher than 100 m^2/g (32, 33). The copper aluminate is not easily reduced as compared with cupric oxide (24, 34, 37). Hence, the peak temperature of 1 wt% Cu/γ-alumina is higher than that of 5 wt% Cu/γ-alumina as shown in Figs, 1b and 1d. Accordingly, the amount of $CuAl_2O_4$ reduced to Cu at 400°C is greater than that reduced at 300°C. This is confirmed by the measurements of copper surface area as shown in Table 1. It also explains why the peak temperature of 1 wt% Cu/γ-alumina is higher than that of 5 wt% Cu/γ-alumina as shown in Figs. 1b and 1d. Therefore, the 1 wt% Cu/γ-alumina catalyst exhibits a stable activity at different temperatures due to the copper aluminate and gives a lower initial activity at 300 or 350°C as compared with that of 1 wt% Cu/YSZ (see Figs. 2 and 3), although its copper dispersion and BET area are higher.

On the other hand, since YSZ is a crystalline oxide (17, 19), it has a very smooth surface and possesses few pores. Hence, at a high enough temperature, the copper atoms supported on YSZ will migrate until they meet and coalesce to form large crystallites which, in order to reduce their surface energy, results in a loss of metal surface area, a decrease in sorptive capacity, and a decrease in catalytic activity. The loss of copper surface area with increased reducing temperatures is shown in Table 1. If the support surface is perfect, i.e., ideal surface, surface migration will be the only way to reduce the surface energy of metal. On the other hand, if there are defects such as surface oxygen vacancies of support, the metal atoms can also reduce their surface energy by dropping into the surface defects (14). The nested atoms which have dropped into the oxygen vacancies are always more stable than the corresponding atoms on ideal surface (14). There-

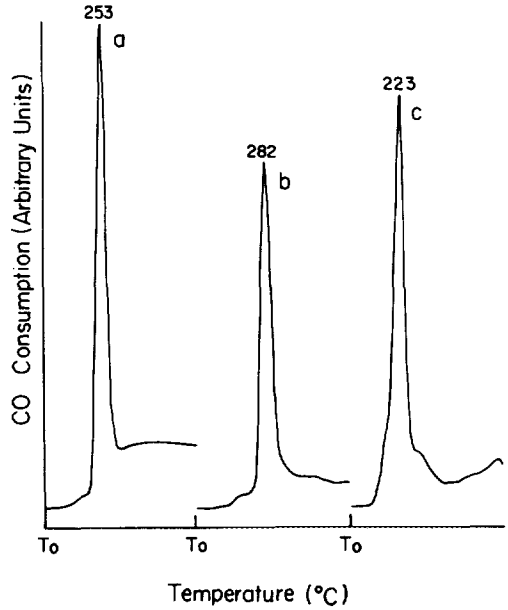

FIG. 7. TPR patterns of 1 wt% Cu/YSZ. Operating conditions are as in Fig. 6. Pretreatment: (a) type IV test at 350°C; (b) type III test at 350°C; (c) reoxidation at 500°C following HTR treatment. Temperature range of TPR, 100°C ($=T_o$) ~500°C.

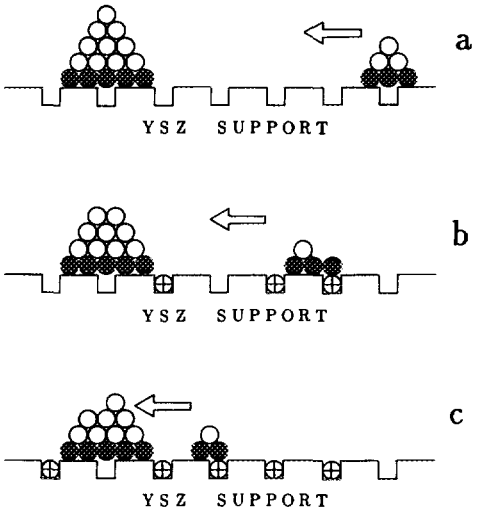

FIG. 8. Migration of copper species on YSZ support. (⊕) Case I copper species; (●) case II copper species; (○) case III copper species; (⊔) oxygen vacancy.

fore, as the copper oxides supported on YSZ are reduced to metallic copper atoms, their behavior may be described as shown in Fig. 8, and is disussed below.

It is conceivable that the copper oxide support on YSZ may have different particle sizes. During the reduction at 300 or 350°C, the copper oxide with small particle size will be reduced first and then migrate toward large particles as shown in Figs. 8a and 8b. This is the usual mechanism of sintering (1). During migration, the copper atoms will meet the oxygen vacancies of YSZ and drop into the vacancies as discussed above. This phenomenon has been called "metal nesting" (14). Finally, these particles encounter and agglomerate to cause a decrease in active surface area as shown in Fig. 8c.

4.2. Valence Variation of Copper Species during Reaction

During reaction on 1 wt% Cu/YSZ catalyst, there may exist three copper species as illustrated in Fig. 8. The case I copper indicates the species which has dropped into the nest vacancy; the case II copper indicates the species which locates at the three phase boundary (copper species, YSZ, and gas phases) and interacts more easily with nest vacancy; the case III copper indicates the species which does not contact directly with the YSZ support. The case III copper may be zero valent, monovalent, or divalent depending on the gas phase condition. On the other hand, since there is one or more nest vacancy existing beside the case II copper, its valence does not change depending only on the atmospheric condition.

The oxygen vacancies can catch and reversibly discharge the atomic oxygen which has been adsorbed on the neighboring active metal (3, 38). This action can be described as

$$O_2 + 2^* \rightleftharpoons 2O^* \quad [1]$$

$$O^* + V_o \rightleftharpoons O_o + ^*, \quad [2]$$

where * denotes the active site on case II copper species, V_o denotes the F center of YSZ, which is formed when oxygen vacancy captures two electrons and O_o denotes the lattice oxygen of YSZ.

Once the case II copper at the three phase boundary becomes monovalent, i.e., in Cu_2O, it can no longer be easily reduced or oxidized because of the existence of oxygen vacancies. In other words, the oxygen vacancy can "protect" the interfacial Cu_2O from further reduction or oxidation. This effect is explained as follows.

For the reduction of Cu_2O, as CO approaches Cu_2O, one of the following two paths may occur.

(a) CO is adsorbed on Cu_2O:

$$CO + Cu_2O \rightleftharpoons Cu_2O \cdots CO_{(ad)}. \quad [3]$$

(b) CO reacts with the lattice oxygen:

$$CO + O_o \rightleftharpoons CO_2 + V_o. \quad [4]$$

Once the adsorption step [3] occurs, one of the following three reactions may proceed.

(c) Cu_2O is reduced by $CO_{(ad)}$:

$$Cu_2O \cdots CO_{(ad)} \rightarrow 2Cu + CO_2. \quad [5]$$

(d) $CO_{(ad)}$ reacts with the lattice oxygen:

$$Cu_2O \cdots CO_{(ad)} + O_o \rightarrow Cu_2O + CO_2 + V_o, \quad [6]$$

which is the so-called "metal–support interfacial reaction" (3).

(e) $CO_{(ad)}$ reacts with the adsorbed oxygen:

$$Cu_2O \cdots CO_{(ad)} + O^* \rightarrow Cu_2O + CO_2 + ^*. \quad [7]$$

Hence, the interfacial Cu_2O which locates at the three phase boundary cannot be easily reduced by CO because the adsorbed CO on these Cu_2O can be rapidly removed via reaction [6] as well as reaction [7]. In fact, reactions [1] and [2] can occur at low temperature, even below 250°C (39–42). This suggests that the lattice oxygen required for reaction [6] can be supplied at low temperature. Therefore, the metal–support interfacial reaction via reaction [6] should be able to consume most of the adsorbed CO before the interfacial Cu_2O is reduced by it.

For the oxidation of Cu_2O, as oxygen approaches Cu_2O, one of the following two paths may occur.

(f) Oxygen is adsorbed on Cu_2O:

$$O_2 + 2Cu_2O \rightleftharpoons 2Cu_2O \cdots O_{(ad)}. \quad [8]$$

(g) Oxygen is caught by the oxygen vacancies:

$$O_2 + 2V_o \rightleftharpoons 2O_o. \quad [9]$$

If the adsorption step [8] is established, one of the following three paths may proceed.

(h) Cu_2O is oxidized by $O_{(ad)}$:

$$Cu_2O \cdots O_{(ad)} \rightarrow 2CuO. \quad [10]$$

(i) $O_{(ad)}$ is caught by an oxygen vacancy in the vicinity of Cu_2O:

$$Cu_2O \cdots O_{(ad)} + V_o \rightarrow Cu_2O + O_o. \quad [11]$$

(j) $O_{(ad)}$ reacts with the adsorbed CO:

$$Cu_2O \cdots O_{(ad)} + CO^* \rightarrow Cu_2O + CO_2 + *. \quad [12]$$

In fact, reactions [11] and [12] are similar to reactions [2] and [7], respectively. Hence, the adsorbed oxygen on interfacial Cu_2O can be easily withdrawn by reaction [11] at temperature below 250°C as well as reaction [12]. XRD has confirmed that reaction [10] does not proceed easily (43) and occurs at 400°C under oxygen atmosphere [44]. On the other hand, it has been found (45) that reaction [12] can occur at temperatures below 140°C. Hence, as soon as the interfacial Cu_2O is formed, it can not be oxidized easily. This behavior, that the oxygen vacancy can adjust to the local oxygen concentration depending on gas phase condition, is equivalent to that of oxygen storage (16, 46).

Considering the chemisorptive character of CO, it prefers to adsorb on *p*-type semiconducting oxide (47, 48) due to the lone pair of electrons on carbon, which has a high degree *p* character and results in a donor-type chemisorptive behavior (49). Accordingly, the *p*-type semiconducting oxide, such as Cu_2O (50, 51), which can supply the electron holes, will give a higher activity for the donor-type reaction of CO. In addition, since the Tammann temperature of metallic copper is lower than that of Cu_2O, the metallic copper should be sintered more easily than Cu_2O. Moreover, CO prefers to adsorb on Cu^+ (45, 52, 53) rather than Cu^0 (52, 54). Therefore, Cu^+ should be the most active species among Cu^0, Cu^+, and Cu^{2+} for CO oxidation. Accordingly, the activity of 1 wt% Cu/YSZ should be continuously increased with time if there is a durative formation of the interfacial Cu_2O as discussed above. This effect has been confirmed by the results of Figs. 5 and 7 and will be explained in Section 4.5.

4.3. Effect of Oxygen Vacancy on Dispersion of Copper Oxide

According to Sanchez and Gazquez (14), the nested metal atoms can penetrate further into the crystal structure of the oxide support when the temperature is high enough. Indeed, it has been demonstrated that copper can dissolve in YSZ at elevated temperature (55). It is thus believed that when 1 wt% Cu/YSZ is reduced at 800°C, copper atoms will penetrate into the bulk oxygen vacancies of YSZ via the surface nest vacancies. The mechanism of penetration is illustrated in Figs. 9–11.

Figure 9 shows the adsorption type of CO molecule on CuO/YSZ when the gas phase contains only CO or when oxygen is deficient. Adsorption behavior of this type has been found in many studies (2, 3, 7, 9). Once adsorption of this type occurs, the nest vacancy is occupied by the adsorbed CO molecule, which leads to interference in reaction [2], and the case II copper may thus be reduced to metallic copper. This atomic copper can thereupon drop into the nest vacancy as illustrated in Figs. 10a and 10b. At this moment, if the temperature is raised to an elevated one, bulk penetration of copper atoms may take place. Moreover, as reduction proceeds, the density of the crystallite increases, and, since the metallic copper adheres strongly to the surface through the oxygen vacancy, a tensile stress should develop in the crystallite. This may result in one or more cracks, preferentially at the grain boundaries in the particle. As a result, the copper particle will be split into several parts as shown in Fig. 10c. In general, the larger the particle size is, the more difficult it will become to split. On IrO_2/SiO_2 and Rh_2O_3/SiO_2 catalysts, Wang and Schmidt (56, 57) have proposed a similar concept, that metal oxide may be fissured to small metallic crystallites due to reduction.

According to these discussions, after the HTR pretreatment, small copper particles may penetrate completely into YSZ via nest vacancies as shown in Figs. 11a, 11b, and 11c. After the reoxidation treatment, the copper atoms in the sublayer of YSZ may be enriched back to the surface and completely segregated from the oxygen vacancies (14), as shown in Fig. 11d. However, the copper atoms which have been dissolved in the bulk of YSZ may

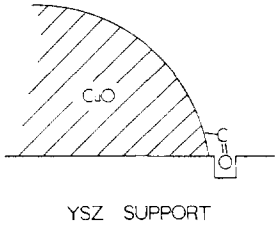

FIG. 9. Adsorption type of CO under oxygen free or oxygen deficient condition.

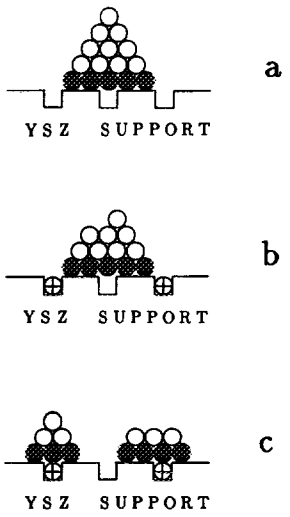

FIG. 10. Split mechanism of copper oxide of small particle size. Symbols are as in Fig. 8.

not return to the surface (see next section). Consequently, with a comparison of Figs. 11a and 11d, the dispersion of the reoxidized catalyst is higher than that of the fresh one. The redispersion of copper oxide by reoxidation has also been observed in our previous work over CuO/Al_2O_3 (21).

Considering Fig. 11b, the copper species has a strong interaction with YSZ support due to the effect of anchorage (14), whereas there is no such strong interaction in the case of Figs. 11a and 11d. In general, the copper species which possesses a strong interaction with support will be more stable than that without such interaction and hence give a high temperature peak in TPR measurement (34, 37). Therefore, we speculate that the peak temperature of the copper species which is indicated in Fig. 11b should be higher than those shown in Figs. 11a and 11d. In addition, the peak temperature of the catalyst, as in Fig. 11d, should be lower than that of the fresh catalyst (Fig. 11a) owing to its higher dispersion.

Indeed, the TPR patterns agree with the above suggestions. From the comparison of Figs. 6a, 7b, and 7c, the peak of the HTR-treated catalyst shifts toward higher temperature as compared with that of the fresh catalyst (Fig. 6a), whereas that of the reoxidized catalyst shifts toward lower temperature. Therefore, as lower peak temperature indicates higher dispersion, it is seen that reoxidation treatment leads to redispersion. The proposed scheme, shown in Fig. 11, is also confirmed.

4.4. Activity Test under Oxygen Lean Condition

After reduction at 800°C, some metallic copper crystallites, especially small ones, may penetrate into YSZ, and the surface-residual copper atoms may have serious sintering. Hence, no activity is observed in the type II test at 300°C, as shown in Fig. 4. When the temperature is raised to 350°C, a few copper atoms may be reoxidized to form Cu_2O under the oxygen deficient condition. Hence, the rapid increase in activity at 350°C, as shown in Fig. 4, is attributed to the increase of surface copper species due to the copper enrichment from the sublayer of YSZ and the formation of Cu_2O.

As the temperature is maintained at 400 or 450°C, the enriched and surface-residual copper atoms begin migration because the nest vacancies are still occupied by copper atoms. Therefore, in association with the discussion of Section 4.1, the deactivation with time at 400 or 450°C, as shown in Fig. 4, is due to sintering of copper atoms, although some bulk Cu_2O, which has been confirmed by CO-TPR (Fig. 6c), still exists.

In order to ascertain the bulk penetration of copper atoms after reduction at 800°C, the XRD measurements were carried out and the results are shown in Fig. 12. There is no diffraction peak for copper species. The peaks of YSZ shown in Figs. 12b and 12c shift systematically toward lower diffraction angles as compared with that in Fig. 12a. According to Bragg's law (58) and the *d*-spacing formula, these shifts of diffraction angles infer that the bulk oxygen vacancies of YSZ are replaced by copper atoms which cause expansion of the unit cell of YSZ

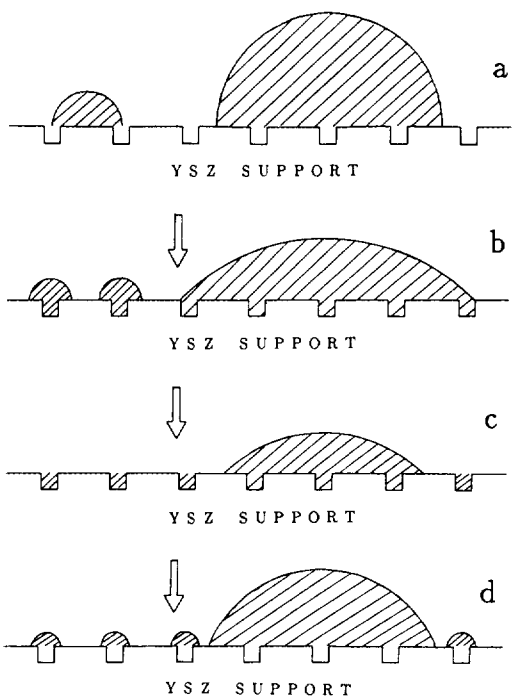

FIG. 11. Proposed scheme for the effect of oxygen vacancy on dispersion of supported copper species. (a) Fresh catalyst under oxygen rich condition, T = 300 ~ 350°C; (b) HTR pretreated catalyst under oxygen rich condition, T = 400 ~ 450°C; (c) after HTR treatment at 800°C; (d) reoxidation in air at 500°C following HTR treatment.

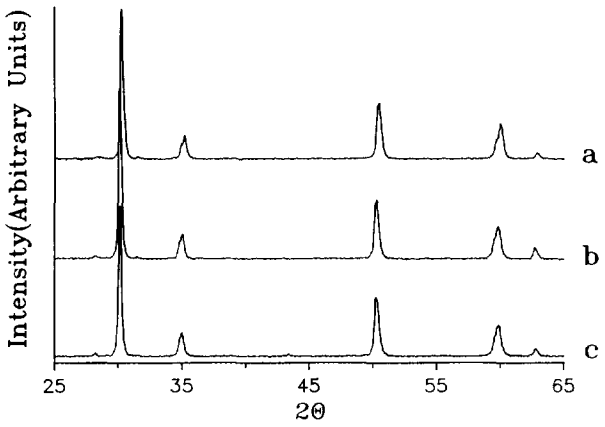

FIG. 12. XRD spectra of 1 wt% Cu/YSZ catalyst. Pretreatment: (a) fresh; (b) HTR; (c) reoxidation.

crystal. Recently, Zou and Petric (59) also observed a shift toward lower diffraction angles when yttrium atoms are doped into lithium zirconate.

Under the condition of the type I test, most of the nest vacancies are vacant at the outset and all copper species should be cupric oxide due to fresh catalyst. Therefore, several reactions as follows may occur.

$$O_2 + 2^* \rightleftharpoons 2O^* \quad [1]$$

$$O^* + V_o \rightleftharpoons O_o + * \quad [2]$$

$$CO + CuO^{\langle 2\rangle} \rightleftharpoons CuO^{\langle 2\rangle} \cdots CO_{(ad)} \quad [13]$$

$$CuO^{\langle 2\rangle} \cdots CO_{(ad)} \rightarrow Cu^{\langle 2\rangle} + CO_2 \quad [14]$$

$$CuO^{\langle 2\rangle} \cdots CO_{(ad)} + O^* \rightarrow CuO^{\langle 2\rangle} + CO_2 + * \quad [15]$$

$$CuO^{\langle 2\rangle} \cdots CO_{(ad)} + O_o \rightarrow CuO^{\langle 2\rangle} + CO_2 + V_o, \quad [16]$$

where superscript ⟨2⟩ denotes the case II copper species.

The TPR result as shown in Fig. 6d has confirmed that most of CuO supported on YSZ can be directly reduced to Cu during the type I test at 300°C. This agrees with the result that the reduction of CuO to Cu may be direct at temperatures below 200°C without two steps, i.e., $Cu^{2+} \rightarrow Cu^{+} \rightarrow Cu^{0}$ (30, 43, 60, 61), and coincides with the results discussed in Secion 4.3. Therefore, reaction [14] proposed in the mechanism is confirmed.

The high initial activities at 300 or 350°C as shown in Fig. 3 are due to a combination of reactions [14]–[16]. The cupric oxide species beside the nest vacancies are gradually reduced to copper atoms which then fill in the nest vacancies. This leads to the interruption of reactions [2] and [16]. Consequently, CO consumption is curtailed. Moreover, once the nest vacancies are filled, the reduced copper atoms begin migration, agglomeration, and then sintering. Therefore, the activity at 300 and 350°C decreases with time. This has been confirmed by the TPR result of Fig. 6d which indicates that large amounts of metallic copper had been formed after the type I test at 300°C for 27 h. The first peak of Fig. 6d can be ascribed to the oxygen which is strongly and irreversibly adsorbed on metallic copper and results in a temperature-programmed reaction with CO during the TPR. The strong and irreversible adsorption of oxygen on metallic copper has also been found and demonstrated by Vannice and co-workers over Cu/Al_2O_3 (45) and Cu/SiO_2 (62), respectively. They concluded (62) that the irreversibly adsorbed oxygen on Cu can increase from near zero at 77 K to that corresponding to bulk Cu_2O formation at 473 K. However, the amount of bulk Cu_2O seems to be small under our conditions. In fact, many studies (3, 8, 9, 28, 63) have verified that the interfacial reaction, such as reaction [16], can have a large contribution for CO oxidation over Pt and Pd catalysts. That is to say, the occurrence of reaction [16] can markedly enhance the activity of 1 wt% Cu/YSZ and leads to the higher initial activity during the type I test at 300°C.

In the type I test at 400 or 450°C, the mild increase in activity with time after 5 h is ascribed to the improvement of dispersion as well as the formation of Cu_2O, which has been confirmed by the TPR pattern of Fig. 6b. This is because the copper atoms can begin penetration at 400 or 450°C as discussed in Section 4.3. This action of penetration that causes the metal atoms to spread and prevent their further migration and sintering is similar to an effect of anchorage (14). Moreover, since the migration of copper atoms occurs before penetration, deactivation is observed in the first 3 h at 400 or 450°C, as shown in Fig. 3.

Comparing the steady state activities of Figs. 3 and 4, the explanation as mentioned above can be further corroborated. Since all of the nest vacancies can be filled by atomic copper which is produced during reaction or by HTR pretreatment the steady state conversions at 300 and 350°C have the tendency to approach the same. This means that once the effect of oxygen vacancy is taken away, the activity depends only on metallic copper. On the other hand, when both the bulk oxygen vacancy and the nest vacancy are occupied by atomic copper due to HTR pretreatment, the penetration effect is stemmed at 400 and 450°C without improvement in dispersion. Hence, the peak temperature of Fig. 6c is higher than that of Fig. 6b owing to its low dispersion. This may clarify that the penetration effect due to the bulk oxygen vacancy can enhance the activity at higher temperatures.

4.5. Activity Tests under Oxygen Rich Condition

During the type III test at 300°C, negligible activity in the first half-hour may be considered as an induction pe-

riod which is due to strong adsorption of oxygen on metallic copper. This phenomenon has also been found by Severino and Laine over unsupported CuO (64) and has been attributed to the same reason. This agrees with the result of Leon y Leon and Vannice (62), that oxygen can be adsorbed more strongly and irreversibly on metallic copper than CO, and with that of Choi and Vannice (45), that oxygen can strongly adsorb on Cu and block CO adsorption leading to a decrease in activity of Cu/Al_2O_3 for CO oxidation. Following this period, the drastic increase in activity can be attributed to the formation of Cu_2O due to kinetic favor (43, 61, 62) and some improvement in dispersion because of oxygen rich conditions. After 7 h, the gradual deactivation is attributed to the appearance of CuO, which ultimately leads to a stable activity due to thermodynamic favor (44, 61) and oxygen rich condition. For the type III test at 350°C, the continuous increase in activity is due to the fact that the amounts of exposed copper atoms can be increased by means of enrichment as mentioned in Section 4.3.

In the type IV test, the surface state of the catalyst is described as in Fig. 11a where all nest vacancies are free. Hence, the continuous activity enhancement is attributed to the effect of oxygen vacancies on protecting interfacial Cu_2O, as discussed in Section 4.2. As the case II copper is transformed to Cu_2O gradually, the activity is increased with time. In addition, reaction [6] can thus be introduced to enhance the total reaction rate of this catalyst. On the other hand, for CO + NO reaction over an oxygen-ion conducting support (16), higher temperature leads to more significant activity enhancement, and this can be attributed to the oxygen transport characteristics on the support surface. At lower temperature the oxygen mobility is also lower; hence the rate of reaction [2] is decreased and reaction [6] may thereupon be inhibited. Therefore, the sustained increase in activity with time at 300°C is less obvious than that at 350°C.

Recently, many reports (8, 9, 28, 63) have verified that the metal–support interfacial reaction, such as reaction [6], can certainly enhance the catalytic activity of Pt and Pd catalysts for CO oxidation. In particular, many studies (3, 39, 40, 46, 65–68) which employ a solid electrolyte cell and an open-circuit potential system have substantiated the existence of such metal–support interfacial reaction on Pt/YSZ for CO oxidation by finding the formation of mixed potential. Hetrick and Logothetis (66) and Yentekakis *et al.* (68) have also demonstrated that a maximum rate of CO oxidation on Pt/YSZ is accompanied by the appearance of the mixed potential. In view of the volcano principle (50), since a pertinent and compatible chemisorption, in which CO is adsorbed on Cu_2O and O_2 is adsorbed on oxygen vacancy, can be established, the sustained increase in activity with the run time in type IV test may be ascribed to the contributions of both the formation of interfacial Cu_2O and the metal–support interfacial reaction.

However, these Cu_2O species exist only at the three phase boundary and it is not easy to produce a TPR peak. Furthermore, using CO as a reducing gas, the curve of TPR pattern usually cannot return to the base line because the Boudouard reaction, i.e., $2CO \rightarrow C + CO_2$, may occur under high temperature (24, 69). Additionally, the tailing of TPR peak is also severe (24). Nevertheless, in Fig. 7a, the plateau near 400°C is the largest and highest of all TPR peaks. This is presumably caused by these interfacial Cu_2O species.

Considering the steady state activities of Fig. 5, the better activity of fresh catalyst may exactly display the importance of metal–support interfacial reaction, i.e., reaction [6], and the interfacial Cu_2O. In the type III test, the state of the HTR pretreated catalyst may be represented by the state shown in Fig. 11c returning to that shown in Fig. 11b. That is to say, however, the nest vacancies are always blocked by the atomic copper during the type III test. This leads to the disappearance of reactions [2], [4], [6], [11], and [16]. In other words, if there is no effect of oxygen vacancy such as penetration effect at high temperature, formation of interfacial Cu_2O, and metal–support interfacial reaction, the steady state activity should be the same. This is confirmed by the results of Figs. 3 and 4 at 300 and 350°C.

5. CONCLUSIONS

The effects of oxygen vacancies of YSZ support on CO oxidation over copper catalyst are dependent on the pretreatment of catalyst and the gas phase conditions of reaction.

1. Under oxygen lean conditions the HTR pretreated catalyst exhibits no or low activity. This is caused by the penetration of copper atoms into the oxygen vacancies during HTR pretreatment. The strong deactivation of the fresh catalyst with time at 300 and 350°C can be explained by the sintering of copper atoms, whereas a mild increase in activity at 400 or 450°C is due to copper atoms dropping into the nest vacancies and thus resulting in split of the copper crystallites.

2. Under oxygen rich conditions the HTR pretreated catalyst shows a drastic reappearance of activity. This may be caused by the enrichment of copper atoms from the YSZ sublayer to the YSZ surface and the formation of some bulk Cu_2O. A durative activity enhancement of the fresh catalyst is attributed to the formation of interfacial Cu_2O and the metal–support interfacial reaction.

This work demonstrates that the geometric IMSI can improve the dispersion of base metal and enhance the

activity of base metal oxide, and that the oxygen vacancies of YSZ can protect the interfacial Cu_2O which leads to a significant activity enhancement.

It is believed that if a high BET area YSZ can be developed, an outstanding performance of CuO/YSZ for CO oxidation can be obtained owing to the extension of three phase boundary line. This is studied in our further work.

ACKNOWLEDGMENTS

This work was supported by the National Science Council of Republic of China under Contract NSC 83-0402-E-007-006. We thank Professor C.-T. Yeh for providing the TCD equipment of H_2-TPR and Mr. Y.-P. Wang for carrying out the XRD measurements.

REFERENCES

1. Stevenson, S. A., Dumesic, J. A., Baker, R. T. K., and Ruckenstein, E., Eds., "Metal–Support Interaction in Catalysis, Sintering, and Redispersion." Van Nostrand–Reinhold, New York, 1987.
2. Burch, R., and Flambard, A. R., *J. Catal.* **78,** 389 (1982).
3. Metcalfe, I. S., and Sundaresan, S., *AIChE J.* **34,** 195 (1988).
4. Naraynan, S., *J. Sci. Ind. Res.* **44,** 580 (1985).
5. Bell, A. T., *in* "Catalyst Design, Progress and Perspectives" (L. L. Hegedus *et al.*, Eds.), p. 103. Wiley, New York, 1987.
6. Haller, G. L., and Resasco, D. E., *Adv. Catal.* **36,** 173 (1989).
7. Vannice, M. A., and Sudhakar, C., *J. Phys. Chem.* **88,** 2429 (1984).
8. Jin, J., Okuhara, T., Mains, G. J., and White, J. M., *J. Phys. Chem.* **91,** 3310 (1987).
9. Lööf, P., Kasemo, B., Andersson, S., and Frestad, A., *J. Catal.* **130,** 181 (1991).
10. Sayle, T. X. T., Parker, S. C., and Catlow, C. R. A., *J. Chem. Soc., Chem. Commun.*, 977 (1992).
11. Munuera, G., Fernandez, A., and Gonzalez-Elipe, A. R., *in* "Catalysis and Automotive Pollution Control II" (A. Crucq, Ed.), p. 207. Elsevier, Amsterdam, 1991.
12. Jackson, N. B., and Ekerdt, J. G., *J. Catal.* **101,** 90 (1986).
13. Silver, R. G., Hou, C. J., and Ekerdt J. G., *J. Catal.* **118,** 400 (1989).
14. Sanchez, M. G., and Gazquez, J. L., *J. Catal.* **104,** 120 (1987).
15. Shpiro, E. S., Dysenbina, B. B., Tkachenko, O. P., Antoshin, G. V., and Minachev, K. M., *J. Catal.* **110,** 262 (1988).
16. Cho, B. K., *J. Catal.* **131,** 74 (1991).
17. Subbarao, E. C., Ed., "Solid Electrolytes and Their Applications." Plenum, New York, 1980.
18. Etsell, T. H., and Flengas, S. N., *Chem. Rev.* **70,** 339 (1970).
19. Gellings, P. J., and Bouwmeester, H. J. M., *Catal. Today* **12,** 1 (1992).
20. Engel, T., and Ertl, G., *Adv. Catal.* **28,** 1 (1979).
21. Huang, T.-J., Yu, T.-C., and Chang, S.-H., *Appl. Catal.* **52,** 157 (1989).
22. Huang, T.-J., and Yu, T.-C., *Appl. Catal.* **71,** 275 (1991).
23. Kummer, J. K., *Prog. Energy Combust. Sci.* **6,** 177 (1980).
24. Severino, F., Brito, J., Carias, O., and Laine, J., *J. Catal.* **102,** 172 (1986).
25. Evans, J. W., Wainwright, A. J., Bridgewater, A. J., and Young, D. J., *Appl. Catal.* **7,** 75 (1983).
26. Chang, T.-C., Chen, J.-J., and Yeh, C.-T., *J. Catal.* **96,** 51 (1985).
27. Summers, J. C., and Ausen, S. A., *J. Catal.* **58,** 131 (1979).
28. Oh, S. H., and Eickel, C. C., *J. Catal.* **112,** 543 (1988).
29. Shimokawabe, M., Asakawa, H., and Takezawa, N., *Appl. Catal.* **59,** 45 (1990).
30. Robertson, S. D., McNicol, B. D., De Baas, J. H., Kloet, S. C., and Jenkins, J. W., *J. Catal.* **37,** 424 (1975).
31. Van der Grift, C. J. G., Mulder, A., and Geus, J. W., *Appl. Catal.* **60,** 181 (1990).
32. Friedman, R. M., Freeman, J. J., and Lytle, F. W., *J. Catal.* **55,** 10 (1978).
33. Strohmeier, B. R., Leyden, D. E., Field, R. S., and Hercules, D. M., *J. Catal.* **94,** 514 (1985).
34. Dumas, J. M., Geron, C., Kribii, A., and Barbier, J., *Appl. Catal.* **47,** L9 (1989).
35. Keoppel, R. A., Baiker, A., and Wokaun, A., *Appl. Catal. A General* **84,** 77 (1992).
36. Delk II, F. S., and Vàvere, A., *J. Catal.* **85,** 380 (1984).
37. Gentry, S. J., and Walsh, P. T., *J. Chem. Soc., Faraday Trans. 1* **78,** 1515 (1982).
38. Etsell, T. H., and Flengas, S. N., *J. Electrochem. Soc.* **118,** 1890 (1971).
39. Okamoto, H., Obayashi, H., and Kudo, T., *Solid State Ionics* **3/4,** 453 (1980).
40. Okamoto, H., Kawamura, G., and Kudo, T., *J. Catal.* **82,** 332 (1983).
41. Saranteas, C., and Stoukides, M., *J. Catal.* **93,** 417 (1985).
42. Badwal, S. P. S., and Ciacchi, F. T., *J. Appl. Electrochem.* **16,** 28 (1986).
43. Pierron, E. D., Rashkin, J. A., and Roth, J. F., *J. Catal.* **9,** 38 (1967).
44. Yanase, A., and Komiyama, H., *Surf. Sci.* **248,** 11 (1991).
45. Choi, K. I., and Vannice, M. A., *J. Catal.* **131,** 22 (1991).
46. Metcalfe, I. S., and Sundaresan, S., *Chem. Eng. Sci.* **41,** 1109 (1986).
47. Bielański, A., and Haber, J., "Oxygen in Catalysis," p. 260. Dekker, New York, 1991.
48. Doshi, R., Alcock, C. B., Gunasekaran, N., and Carberry, J. J., *J. Catal.* **140,** 557 (1993).
49. Orchin, M., and Jaffè, H. H., "The Importance of Antibonding Orbitals," p. 32. Houghton Mifflin, Boston, 1967.
50. Bond, G. C., "Heterogeneous Catalysts: Principles and Applications," 2nd ed. Oxford Univ. Press (Clarendon), London/New York, 1987.
51. Rakhshani, A. E., *Solid-State Electron.* **29,** 7 (1986).
52. Miró, E. E, Lombardo, E. A., and Petunchi, J. O., *J. Catal.* **104,** 176 (1987).
53. Bijsterbosch, J. W., Kapteijn, F., and Moulijn, J. A., *J. Mol. Catal.* **74,** 193 (1992).
54. London, J. W., and Bell, A. T., *J. Catal.* **31,** 32 (1973).
55. Fabry, P., and Kleitz, M., *J. Electrochem. Soc.* **126,** 2183 (1979).
56. Wang, T., and Schmidt, L. D., *J. Catal.* **66,** 301 (1980).
57. Wang, T., and Schmidt, L. D., *J. Catal.* **70,** 187 (1981).
58. West, A. R., "Solid State Chemistry and Its Applications," p. 366. Wiley, New York, 1984.
59. Zou, Y., and Petric, A., *J. Electrochem. Soc.* **140,** 1388 (1993).
60. Voge, H. H., and Atkins, L. T., *J. Catal.* **1,** 171 (1962).
61. Lo Jacono, M., Cimino, A., and Inversi, M., *J. Catal.* **76,** 320 (1982).
62. Leon y Leon, C. A., and Vannice, M. A., *Appl. Catal.* **69,** 269 (1991).
63. Serre, C., Garin, F., Belot, G., and Maire, G., *J. Catal.* **141,** 9 (1993).
64. Severino, F., and Laine, J., *Ind. Eng. Chem. Prod. Res. Dev.* **22,** 396 (1983).
65. Fleming, W. J., *J. Electrochem. Soc.* **124,** 21 (1977).
66. Hetrick, R. E., and Logothetis, E. M., *Appl. Phys. Lett.* **34,** 117 (1979).
67. Okamoto, H., Kawamura, G., and Kudo, T., *J. Catal.* **82,** 322 (1983).
68. Yentekakis, I. V., Neophytides, S., and Vayenas, C. G., *J. Catal.* **111,** 152 (1988).
69. Serre, C., Garin, F., Belot, G., and Maire, G., *J. Catal.* **141,** 1 (1993).